# ORIENTATION STRATEGIES OF AIRBORNE THREE-LINE SCANNER STARIMAGER'S IMAGERY WITH MINIMUM GROUND CONTROL

Tianen CHEN [*], Ryosuke SHIBASAKI [*], Koichi TSUNO[**]

[*] Shibasaki Lab, Institute of Industrial Science, University of Tokyo
4-6-1 Komaba, Meguro-ku, Tokyo 153-8505, JAPAN
chentian@iis.u-tokyo.ac.jp; shiba@skl.iis.u-tokyo.ac.jp
[**] STARLABO Corporation
1-20-1, Sanshin BLDG, Shibuya, Shibuya-ku, Tokyo 150-0002, JAPAN
tsuno-koichi@sei.co.jp

**Commission III, WG III/1**

**KEY WORDS:** Airborne Three-Line-Scanner, Triangulation of TLS Imagery, GPS/INS integration, Minimum GCP, Platform modelling

ABSTRACT:

STARIMAGER is a helicopter-mounted high resolution Three-Line Scanner (TLS) imaging system developed by STARLABO Corporation jointly with the University of Tokyo for large scale mapping, temporary linear ground objects investigation, and remote sensing applications in 2000. As other airborne and spaceborne linear imaging sensors, STARIMAGER is equipped with GPS/IMU to record the exterior orientation parameters of each obtained image line during flight. However, the recorded GPS/IMU data couldn't be used until their some systematic errors such as offsets between GPS antenna and perspective centre, misalignment between IMU axes and camera coordinate system axes, and drifts of IMU with time elapse etc. with similar conventional aerial triangulation. Moreover, to achieve high pointing accuracy with STARIMAGER imagery and minimum ground control points, we tested several orientation strategies including different sensor models, different block configuration and control information with the real flight data and obtained excitement results in this paper. We sure these experimental orientation strategies will be valuable for other future applications with airborne and spaceborne linear imagery.

## 1 Introduction

The increasing demand for up-to-date information in spatially referenced GIS require development of fast, reliable, and accurate acquisition systems. Although the conventional cartographic aerial film cameras have been playing the key role in the mapping field and remote sensing applications during the last decades, their following drawbacks make them away from the modern information technology (Donald, 1996):

- Processing takes time, clean water, and chemicals and produces hard copy not ready for electronic manipulation.
- Processed film must be scanned before it is computer ready, risking scratches on the film original.
- No direct means of confirming that targets being photographed is available.
- Use is limited to available film emulsion and spectral characteristics.

Electro-optical scanners and digital sensors (CCD) have been used for industrial field such as computer vision, remote sensing and some mapping applications since the last seventies due to their certain performance advantages over photographic film-based cameras. For example, digital sensors have higher signal-to-noise ratio under conditions of low scene contrast. This, in effect, takes the low-contrast Earth scene and performs a contrast stretch to enhance the content and interpretability, especially image matching of the imagery. Further advantages, particularly to the military, are that CCD-based arrays are amenable to real-time data transmission (Strunk *et al.*, 1992).

Most spaceborne Earth-orbiting satellites use multispectral digital linear sensors in pushbroom mode to collect Earth surface imagery for stereo-mapping and remote sensing applications since 2D CCD array imaging systems with a comparable size

and resolution have not been available presently and are not likely to be available in the future. For example, SPOT 1, 2, and 3 use the across-orbit technique to collect stereo imagery using pushbroom linear CCD scanners. MOMS-02, IKONOS-2, QuickBird and future SPOT 5 use the along-track technique to collect stereo imagery for mapping.
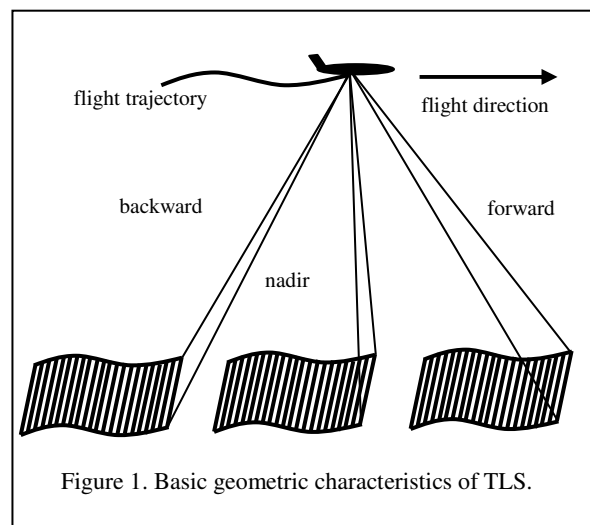


Figure 1. Basic geometric characteristics of TLS.

With advances in satellite and inertial (GPS/INS) georeferencing techniques, some commercial airborne digital sensors have been developed and put into practical applications in last decade. For example, the DPA (Digital Photogrammetry Assambly) was finished and tested by the Institute of Photogrammetry, University of Stuttgart to produce 1:25,000 and 1:50,000 scales maps and automated DTM generation to

accuracies of better than 3m in 1995. The LH Systems ADS40 airborne digital sensor was developed by LH Systems Co. Ltd in 2000 and has been put on the world market. STARLABO Cooperation designed the helicopter-mounted high resolution TLS imaging system STARIMAGER jointly with University of Tokyo in 2000 and have finished several test flights and practical applications. These imaging systems use three linear arrays mounted in the sensor focal plane to collect forward-, nadir-, and backward-looking imagery for stereo mapping. The concept of three linear scanners to collect stereo imagery has been described in many literatures (Chen, 2001; ) and is illustrated in Figure 1.

Unlike frame photography, where all pixels in the image are exposed simultaneously, each line of TLS image is collected in a pushbroom fashion at a different instant of time. Therefore, there is in principle a different set of values for the six exterior orientation elements for each line of the pushbroom scan. Although the traditional indirect approach using ground control points for the determination of the exterior orientation elements of frame photographs through standard aerial triangulation works for frame aerial photographs and spaceborne imagery, this process if highly inefficient. This is because satellite platforms remain relatively stable in relation to their orbital altitude; any deviation of attitude from normal is usually minor and systematically spread over the entire satellite scene (Christensen et al., 1988), so mathematical sensor models are developed to recover the time-dependent position and orientation of the scanner. Airborne scanners on the other hand are subject to atmospheric turbulence during their flight that can lead to severe image distortions in the raw TLS imagery. For airborne TLS a direct processing strategy utilizing direct measurements of the exterior orientation provided by GPS and INS is necessary for operational and efficient data evaluation. Even though direct georeferencing is no must for digital frame cameras a GPS/INS component is also included in some systems (Toth, 1998).

The purpose of this paper is to deal with the integration of GPS, INS, and STARIMAGER imagery for the georeferencing of a digital airborne linear camera system with minimum ground control. In this paper we tested STARIMAGER imagery with a block of six strips and different number and geometric configuration of ground control points and reported our obtained results which could be taken as theorical reference for practical TLS imagery triangulation and other linear imaging system imagery geo-referencing process.

## 2 Combined Bundle Adjustment with GPS/IMU for STARIMAGER

The STARIMAGER is equipped with a GPS/IMU system to record the position and attitude of each image line during the flight. However, like other frame sensor equipped with GPS/IMU, the use of GPS and IMU for line sensor also requires that certain measures be taken before and after the flight because the positions and orientations from GPS/IMU do not refer to the perspective center of the imaging sensor directly. Caused by translational and rotational offsets, the GPS antenna and the center of the inertial system are displaced from the camera. Additionally, the attitudes from GPS/IMU are calculated from the rotation of the IMU body frame defined by the IMU sensor axes to the local level frame. The IMU axes do not coincide with the image coordinate frame. The translational offsets between GPS antenna and perspective center of camera can be determined using conventional terrestrial surveying methods after installation of the system in the aircraft used for the imaging flight. The rotational offsets between the IMU sensor axes and the camera coordinate system cannot be observed via conventional survey methods. Therefore, these rotational offset or misalignment angles between the IMU and camera system

have to be determined with triangulation using a small number of tie and control points similar to conventional aerial frame camera. In addition to these offsets and misalignments, some systematic errors from GPS/IMU such as drifts of IMU should be considered in triangulation. The primary focus of this section is to present mathematical models used in triangulation of STARIMAGER to deal with the systematic errors from GPS/IMU observing data. Therefore, we will first describe the error sources in GPS/IMU and then give two algorithms to remove the systematic offsets for obtaining accurate exterior orientation parameters for STARIMAGER imagery.

### 2.1 GPS/IMU data process

The GPS/IMU data process is an important step towards high quality imagery and accurate measurements derived from it. The timing of IMU recording, GPS recording and CCD line recording must be done using a synchronized clock. This allows the precise registration of each data-recording event. Due to different sampling frequencies of GPS/IMU, a special software was developed to post-process their original data including GSP data re-sampling according to image line record and coordinate system conversion.

As most tests and applications by integrating GPS/IMU systems for geo-reference of image data, the positions and attitudes from GPS/IMU do not refer to the perspective center of the imaging sensor directly (Chen et al., 2001; Lee et al., 2000). Caused by translation and rotation offsets, the GPS antenna and the center of the IMU are displaced from the camera. Additionally, the attitudes from GPS/IMU are calculated from the rotation of the IMU body frame defined by the IMU sensor axes to the local level frame. The IMU axes do not coincide with the image coordinate frame. These offsets have to be taken into account before applying the orientations for the georeferencing of the imagery. The translation offsets are determined using conversional terrestrial surveying methods after installation of the system in the satellite and aircraft used for the photo flights. The rotation alignments between IMU and camera coordinate system cannot be observed via conventional surveying methods. Additionally, there are some drift errors caused by remaining sensor offsets. Therefore, these alignments and drift errors have to be determined with in-flight calibration using a small number ground tie and control points. In next subsection two methods are introduced to determine the offset of GPS, alignments and drift errors of IMU for high accuracy positions and attitudes of images.

### 2.2 Generalized Bundle Adjustment

To relate the image coordinates (x, y) of one point to its mapping coordinates (X, Y, Z), the following collinear equations are used:

$$
\begin{bmatrix} X \\ Y \\ Z \end{bmatrix} = \begin{bmatrix} X_N \\ Y_N \\ Z_N \end{bmatrix} + R(\omega_N, \varphi_N, \kappa_N)(\lambda R_{cam} \begin{bmatrix} x \\ y \\ -f \end{bmatrix} + \begin{bmatrix} \Delta X \\ \Delta Y \\ \Delta Z \end{bmatrix}) \quad (1)
$$

where, $(X_N, Y_N, Z_N, \omega_N, \varphi_N, \kappa_N)$ are the exterior orientation parameters of the $N^{th}$ image line on which the image point in the mapping coordinate, and obtained from GSP and IMU observation values by removing the influence of GPS offsets, IMU alignments and drift errors; $R(\omega_N, \varphi_N, \kappa_N)$ is rotation matrix of IMU to mapping coordinate system; $\lambda$ is scaling factor from image to ground; $R_{cam}$ is rotation matrix of camera to satellite fixed coordinate system and the angles can be obtained from table 1 for PRISM; $(\Delta X, \Delta Y, \Delta Z)$ are offsets between GPS antenna and perspective center of camera in satellite coordinate system and can be obtained from the NASDA, Japan; f is focal length of camera.

Figure 2 Lagrange offset correction curve
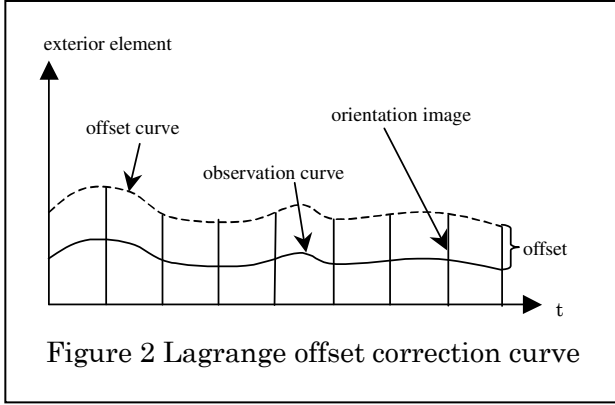
Considering the GSP offset, IMU alignment and drift errors the main factors to influence the accuracy of the exterior orientation $(X_N, Y_N, Z_N, \omega_N, \varphi_N, \kappa_N)$ of the $N^{th}$ image line and taking them as unknown parameters in triangulation we obtain the following model as:

$$\begin{cases} X_N = Z_{GPS} + Z_{offset} \\ Y_N = Z_{GPS} + Z_{offset} \\ Z_N = Z_{GPS} + Z_{offset} \\ \omega_N = \omega_{IMU} + \omega_{alignment} + \omega_{drift} \bullet t \\ \varphi_N = \varphi_{IMU} + \varphi_{alignment} + \varphi_{drift} \bullet t \\ \kappa_N = \kappa_{IMU} + \kappa_{alignment} + \kappa_{drift} \bullet t \end{cases} \quad (2)$$

where, $(X_{GPS}, Y_{GPS}, Z_{GPS})$ are the observation values of GPS antenna in mapping coordinate system; $(\omega_{IMU}, \varphi_{IMU}, \kappa_{IMU})$ are the observation values of IMU in mapping coordinate system; $(X_{offset}, Y_{offset}, Z_{offset})$ are correction values for GPS offsets; $(\omega_{alignment}, \varphi_{alignment}, \kappa_{alignment})$ are correction values for IMU alignments; and $(\omega_{drift}, \varphi_{drift}, \kappa_{drift})$ are correction values for IMU drift errors with time t.

Combining Equation 1 and 2 we can get the extended collinear equation integrating the GSP offset, IMU alignment and drift errors for bundle adjustment as conventional aerial triangulation.

## 3 Test Flight and Experimental Results

In order to check the performance of the camera, the stabilizer, GPS/INS integrated unit, synchronization system, and georeferecing software package, a test site has been established
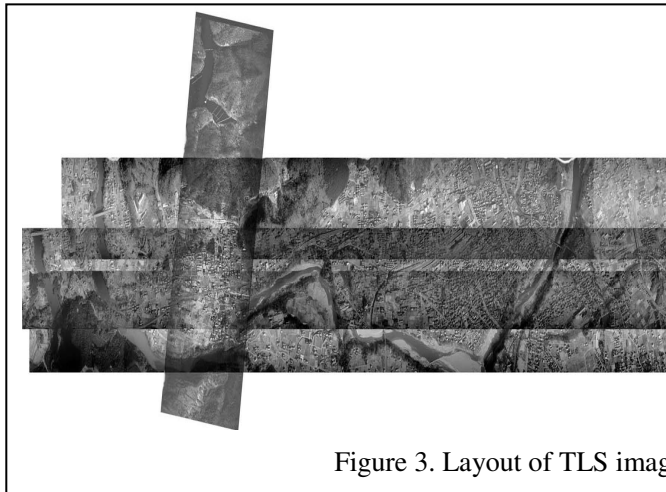


Figure 3. Layout of TLS imagery for triangulation test.

in Yoriityuu, Saitama with more than 120 ground control points over 50 km$^2$. In December 2000 three 10km parallel flight strips

with two 3km cross flight strips of TLS imagery were obtained with STARIMAGER over the test area (Figure 3). More than 30% side overlaps between the three parallel strips are ensured. The following parts will give the test results for different block configurations, different number GCPs used in triangulation and different section lengths of strips.

### 3.1 Single Strip

One obvious character of TLS is a long continues stereo image strip of ground linear objects such as roads, railways, rivers and shore lines etc. could be collected. Single strips are frequently obtained. To ensure geo-referencing accuracy these single strips with reasonable number of ground controls, we tested these strategies:
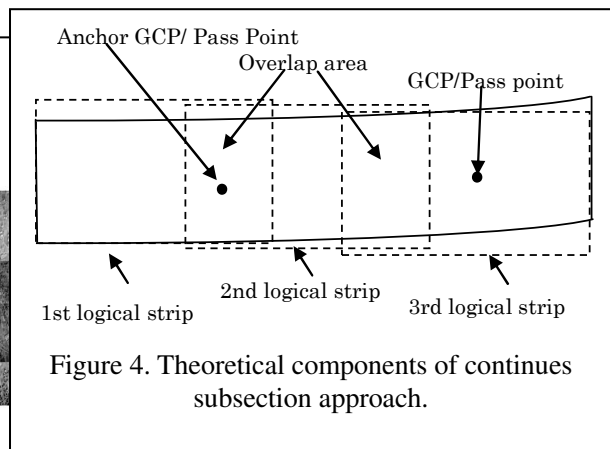
- Different section number
- Different GCP number
- Different GCP configuration

From the 5 single strips we use the middle strip of the three parallel ones as sample to report our tested results based on these strategies. In this strip 30 GCPs and 578 pass points were measured with semi-auto matching method over 10 km length and 0.6 km width.

1) Different section number

Using Equation 2 to compensate GPS/IMU observed data errors for a long strip TLS imagery cannot produce satisfactory results due to some non- systematic or local distortions caused by turbulence of platform. To alleviate this problem we designed a continues subsection approach in the following characters:

- It localizes, and thus simplifies, the complex distortion by logically dividing the entire image strips into a minimal number of logical pieces (Figure 4). Such a division is intuitive and easy to implement. The simplified distortion of each piece can then be modeled using bivariate polynomials with a high accuracy level.

- Since the division is not physical, the continuity of the whole image strip can be retained using the concept of anchor GCPs and pass points. In other words, the whole image strip, after being assembled from the pieces, will form a seamless strip within the framework of the chosen coordinate system.



Figure 4. Theoretical components of continues subsection approach.

| Section Length | RMS_X (m) | RMS_Y (m) | RMS_Z (m) |
|---|---|---|---|
| 20000 | 0.077 | 0.108 | 0.183 |
| 30000 | 0.08 | 0.136 | 0.178 |
| 40000 | 0.099 | 0.18 | 0.183 |
| 50000 | 0.105 | 0.182 | 0.18 |
| 100000 | 0.182 | 0.217 | 0.219 |
| Whole | 0.274 | 0.237 | 0.245 |

Table 1. Statistics associated with different section number.

From this table we find the shorter the subsection, the more accurate the results.

2) Different GCP number

To investigate the influence of GCP number to the final results we tested several cases for the single strip in different section number. Table 2 lists statistics associated with different GCP number for 30000 lines length subcetion.

| GCP Number | RMS_X (m) | RMS_Y (m) | RMS_Z (m) |
|---|---|---|---|
| 2_GCP_A | 0.209 | 0.335 | 0.1806 |
| 2_GCP_B | 0.154 | 0.41 | 0.191 |
| 2_GCP_C | 0.132 | 0.295 | 0.241 |
| 3_GCP_A | 0.158 | 0.339 | 0.187 |
| 3_GCP_B | 0.128 | 0.359 | 0.171 |
| 4_GCP | 0.113 | 0.304 | 0.239 |
| 5_GCP | 0.118 | 0.338 | 0.217 |
| 6_GCP | 0.127 | 0.302 | 0.202 |
| 8_GCP | 0.107 | 0.261 | 0.195 |
| 11_GCP | 0.106 | 0.192 | 0.163 |
| 12_GCP | 0.1 | 0.195 | 0.146 |
| All_GCP | 0.08 | 0.136 | 0.178 |

Table 2. Statistics associated with different GCP number.

From this table we find the more the GCPs in same subsection length, the more accurate the results.

3) Different GCP configuration

We tested several cases of GCP configurations in different subsection length and GCP number, similar conclusion to frame aero images. In general, GCP on corner of blocks or strips can easily produce accurate results.

### 3.2 Multiple Strips

Same test measures as single strip were conducted for the three parallel strips in these strategies:

- Different section number
- Different GCP number
- Different GCP configuration

Total 66 GCPs, 1189 pass points and tie points were measured in semi-auto matching method. Table 3 and 4 list the obtained results in different subsection length and different GCP number.

| Section Length | RMS_X (m) | RMS_Y (m) | RMS_Z (m) |
|---|---|---|---|
| 20000 | 0.066 | 0.083 | 0.179 |
| 30000 | 0.076 | 0.099 | 0.193 |
| 40000 | 0.082 | 0.12 | 0.179 |
| 50000 | 0.079 | 0.13 | 0.172 |
| 100000 | 0.158 | 0.189 | 0.243 |
| Whole | 0.224 | 0.205 | 0.254 |

Table 3. Statistics associated with different section number.

From this table we find the shorter the subsection, the more accurate the results.

| GCP Number | RMS_X (m) | RMS_Y (m) | RMS_Z (m) |
|---|---|---|---|
| 2_GCP_A | 0.123 | 0.144 | 0.224 |
| 2_GCP_B | 0.114 | 0.145 | 0.403 |
| 2_GCP_C | 0.106 | 0.295 | 0.287 |
| 3_GCP_A | 0.198 | 0.241 | 0.223 |
| 3_GCP_B | 0.115 | 0.166 | 0.252 |
| 4_GCP | 0.103 | 0.145 | 0.398 |
| 5_GCP | 0.107 | 0.155 | 0.264 |
| 6_GCP | 0.107 | 0.14 | 0.309 |
| 8_GCP | 0.1 | 0.162 | 0.249 |
| 11_GCP | 0.11 | 0.141 | 0.252 |
| 12_GCP | 0.108 | 0.129 | 0.221 |
| All_GCP | 0.076 | 0.099 | 0.193 |

Table 4. Statistics associated with different GCP number.

From this table we find the more the GCPs in same subsection length, the more accurate the results.

### 3.3 Cross Strips

Based on multi-strip test two cross strips were added into the block for these strategies test:

- Different section number
- Different GCP number
- Different GCP configuration

Total 66 GCPs, 1189 pass points and tie points were measured in semi-auto matching method. Table 5 and 6 list the obtained results in different subsection length and different GCP number.

| Section Length | RMS_X (m) | RMS_Y (m) | RMS_Z (m) |
|---|---|---|---|
| 20000 | 0.064 | 0.08 | 0.168 |
| 30000 | 0.073 | 0.095 | 0.181 |
| 40000 | 0.079 | 0.116 | 0.173 |
| 50000 | 0.075 | 0.123 | 0.164 |

| | | | |
|---|---|---|---|
| 100000 | 0.156 | 0.184 | 0.228 |
| Whole | 0.221 | 0.193 | 0.238 |

Table 5. Statistics associated with different section number.

From this table we find the shorter the subsection, the more accurate the results.

| GCP Number | RMS_X (m) | RMS_Y (m) | RMS_Z (m) |
|---|---|---|---|
| 2_GCP_A | 0.112 | 0.1401 | 0.187 |
| 2_GCP_B | 0.095 | 0.145 | 0.166 |
| 2_GCP_C | 0.107 | 0.136 | 0.226 |
| 3_GCP_A | 0.127 | 0.144 | 0.193 |
| 3_GCP_B | 0.105 | 0.181 | 0.1901 |
| 4_GCP | 0.106 | 0.135 | 0.199 |
| 5_GCP | 0.097 | 0.154 | 0.183 |
| 6_GCP | 0.102 | 0.134 | 0.193 |
| 8_GCP | 0.095 | 0.145 | 0.166 |
| 11_GCP | 0.107 | 0.126 | 0.198 |
| 12_GCP | 0.0907 | 0.124 | 0.217 |
| All_GCP | 0.073 | 0.095 | 0.181 |

Table 6. Statistics associated with different GCP number.

From this table we find the more the GCPs in same subsection length, the more accurate the results.

Comparing Table 3 with 5 and Table 4 with 6 we also find even though the number of GCPs, pass points and tie points are same, the accuracy of planimetry and height for cross strips have been improved considerably due to the geometric conditions have been strengthened.

## 4    Conclusion

The growing demand for fast and accurate data acquisition for mapping and GIS applications requires the provision of new sensors with a high automatic mapping potential as the digital photogrammetry has been widely used to produce various digital mapping data and orthoimages in last decade years. Airborne TLS imaging system has proven the concept of stereo and multi spectral mapping using three-linear pushbroom CCD arrays since 2D CCD array imaging systems with a comparable size and resolution have not been available presently and are not likely to be available in the future. However, these image data collected by the TLS imaging system can only be useful if the geometric relationship between pixels in the images and their corresponding locations on the ground is known. Thus, the determination of the exterior orientation parameters of these time-dependent linear images is the most important problem to be solved firstly. In this paper we provided several orientation strategies to improve the accuracy of point determination with minimum number ground control points. These strategies have been practically applied in STARIMAGER.

## References

Chen, T., and R. Shibasaki, 2001. Development and Calibration of Airborne Three-Line Scanner (TLS) Imaging System, Report on TLS System of STARLABO, IIS, University of Tokyo, Tokyo, Japan, 10 April.

Christensen, E.J., J.R. Jensen, E.W. Ramsey, H.E. Mackley, 1988. Aircraft MSS data registration and vegetation classification for wetland change detection, Photogrammetric Engineering & Remote Sensing, Vol. 53, No. 5 pp. 521-529.

Donald, L. L, 1996. Film Cameras or Digital Sensors ? The Challenge Ahead for Aerial Imaging, Photogrammetric Engineering & Remote Sensing, Vol. 62, No. 3, pp. 285-291.

Lee C., H. J. Theiss, J. S. bethel, and E. M. Mikhail, 2000. Rigorous Mathematical Modeling of Airborne Pushbroom Imaging Systems, Photogrammetric Engineering & Remote Sensing, Vol. 66, No. 4, pp. 385-392.

Strunk, S., J. McMacken, S. Kamasz, W. Washkurak, F. Ma, and S. Chamberlain, 1992. The Development of a Four Million Pixel CCD Imager for Aerial Reconnaissance, Proceedings of the International Society for Optical Engineering, Airborne Reconnaissance XVI, SPIE, 1763:25-36.

Toth, C., 1998. Direct Platform Orientation of Multi-Sensor Data Acquisition Systems, Proceedings of ISPRS Congress Committee IV, Stuttgart, pp. 629-634.